# C-C motif chemokine receptor-like 2 promotes the interferon-γ signaling response in myeloid neoplasms with erythroid differentiation and mutated *TP53*

Nour Sabiha Naji,[1*] Sergiu Pasca,[1*] Theodora Chatzilygeroudi,[1*] Pablo Toledano-Sanz,[2] Joseph Rimando,[3] Yuju An,[1] Yashvi Hemani,[1] Brandy Perkins,[1] Xinghan Zeng,[1] Conover Talbot Jr,[4] Bogdan Paun,[1] Abdulmuez Abdulmalik,[1] Chen Lossos,[5] Tatianna R. Boronina,[6] Ilias Sinanidis,[1] Panagiotis Tsakiroglou,[1] Priyanka Fernandes,[1] Christopher Esteb,[1] Alexander J. Ambinder,[1] Robert N. Cole,[6] Rena Xian,[5] Ivana Gojo,[1] Suman Paul,[1] Mark J. Levis,[1] Amy E. DeZern,[1] Leo Luznik,[7] Styliani Karanika,[8] Linda S. Resar,[9] Richard J. Jones,[1] Frederick Bunz,[10] Lukasz Gondek,[1] Marios Arvanitis[2] and Theodoros Karantanos[1]

[1]Division of Hematologic Malignancies and Bone Marrow Transplantation, Department of Medical Oncology, The Johns Hopkins University School of Medicine, Baltimore, MD; [2]Division of Cardiology, Department of Medicine, Johns Hopkins University, Baltimore, MD; [3]Department of Hematology and Medical Oncology, Emory University School of Medicine, GA; [4]Institute for Basic Biomedical Sciences, Johns Hopkins University, Baltimore, MD; [5]Division of Hematopathology, Department of Pathology, The Johns Hopkins University School of Medicine, Baltimore, MD; [6]Department of Biological Chemistry, Johns Hopkins University, Baltimore, MD; [7]Hematology-Oncology Section, Baylor College of Medicine, Houston, TX; [8]Division of Infectious Diseases, Department of Medicine, The Johns Hopkins University School of Medicine, Baltimore, MD; [9]Division of Hematology, Department of Medicine, Johns Hopkins University, Baltimore, MD and [10]Department of Radiation Oncology and Molecular Radiation Sciences, Johns Hopkins University School of Medicine, Baltimore, MD, USA

*NSN, SPas and TC contributed equally as first authors.*

**Correspondence:** T. Karantanos
tkarant1@jhmi.edu

**Received:** March 4, 2025.
**Accepted:** July 28, 2025.
**Early view:** August 28, 2025.

**https://doi.org/10.3324/haematol.2025.287740**

**A**

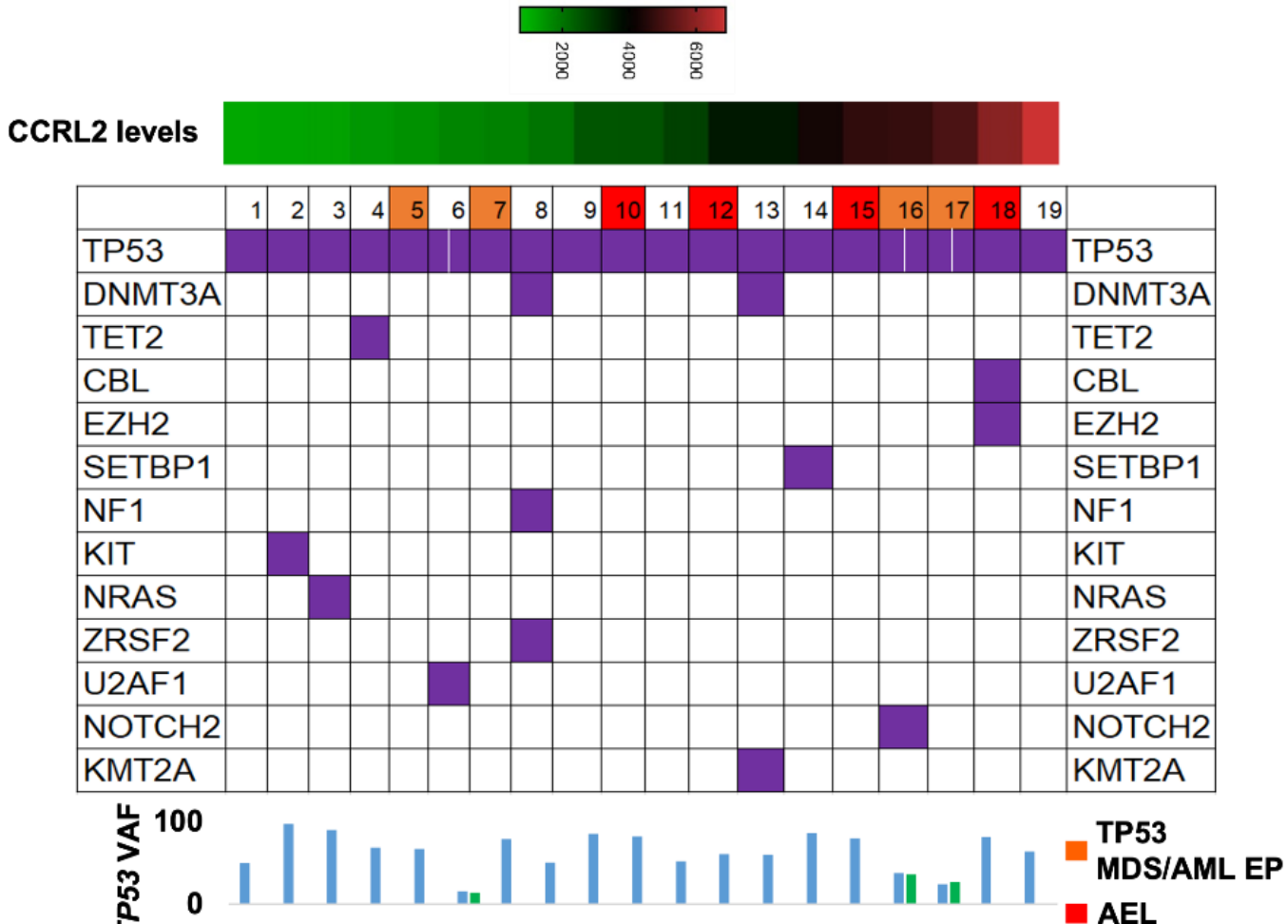


**B**

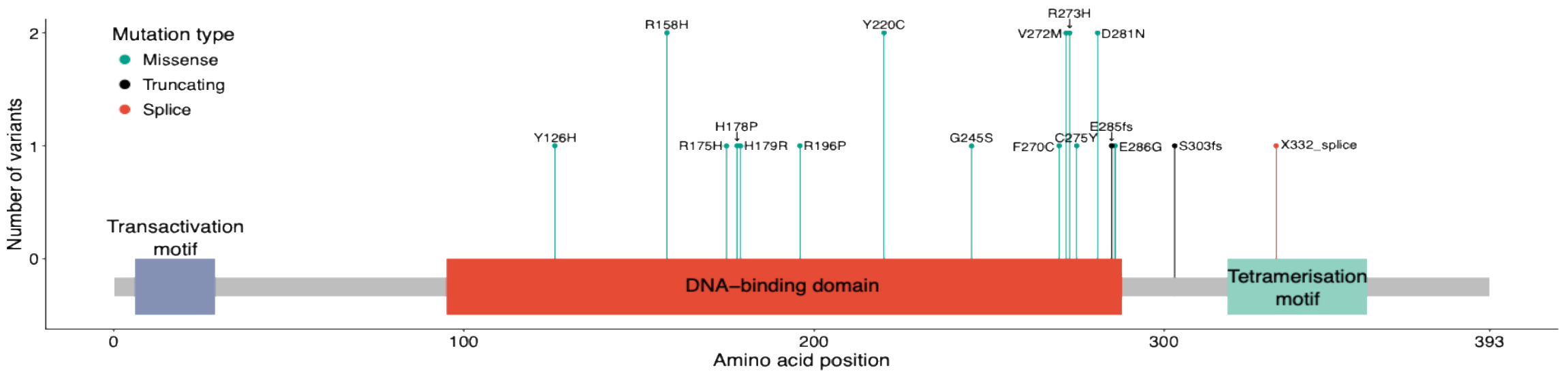


**Supplementary Figure 1**

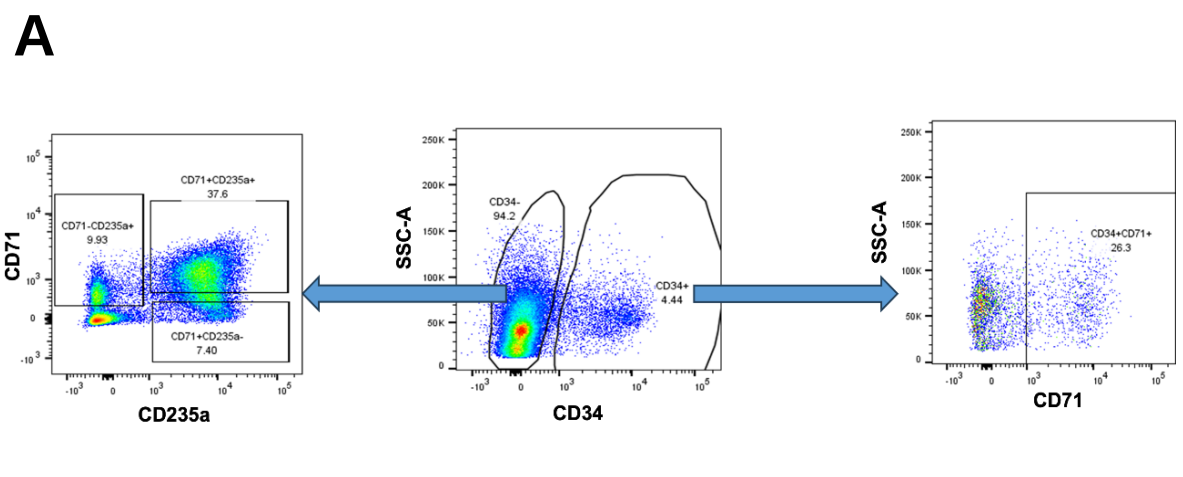


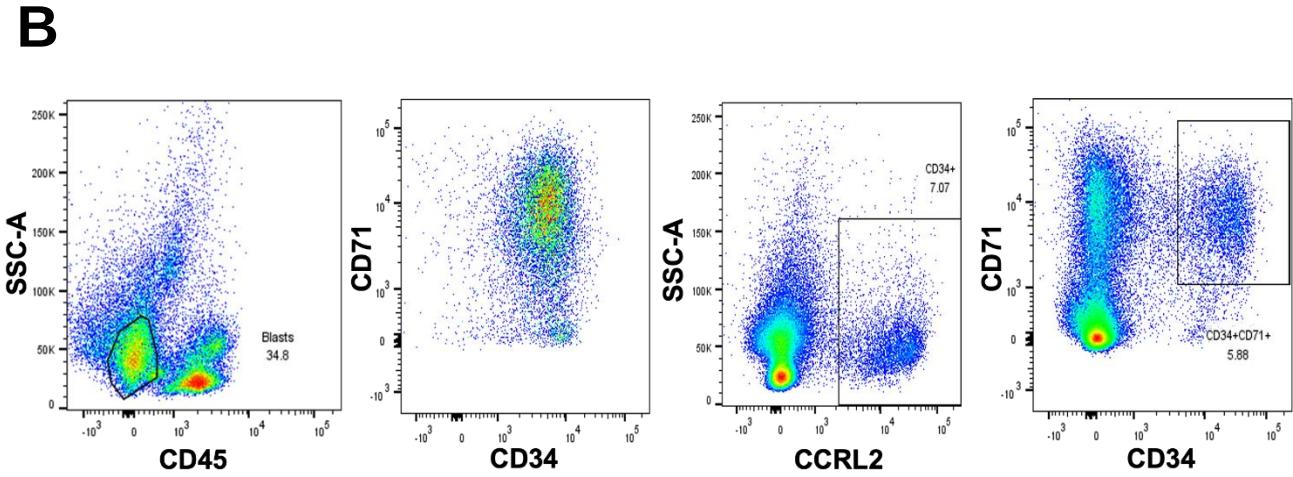


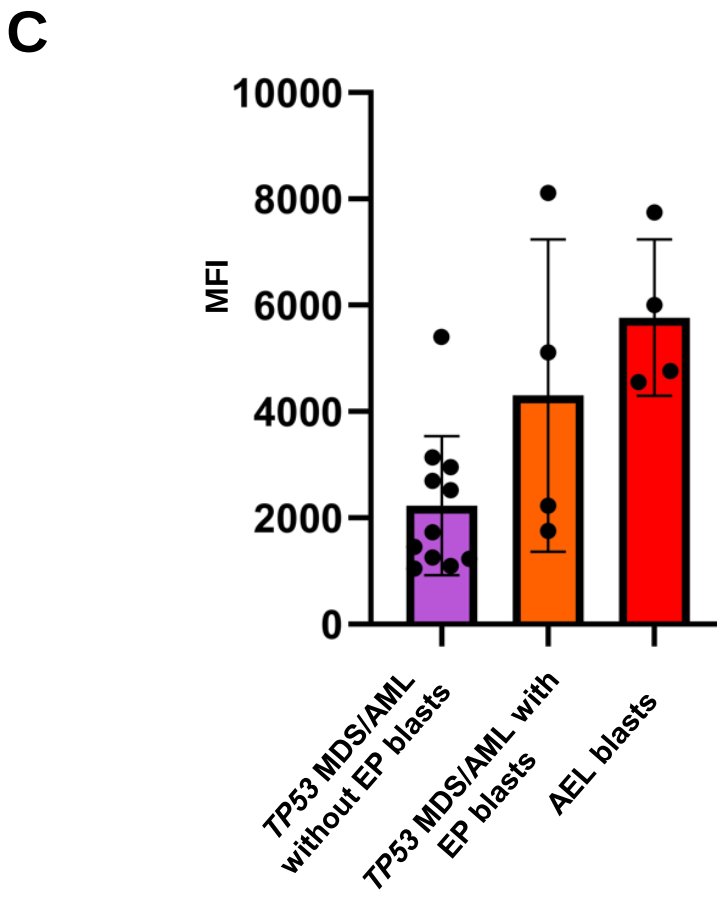


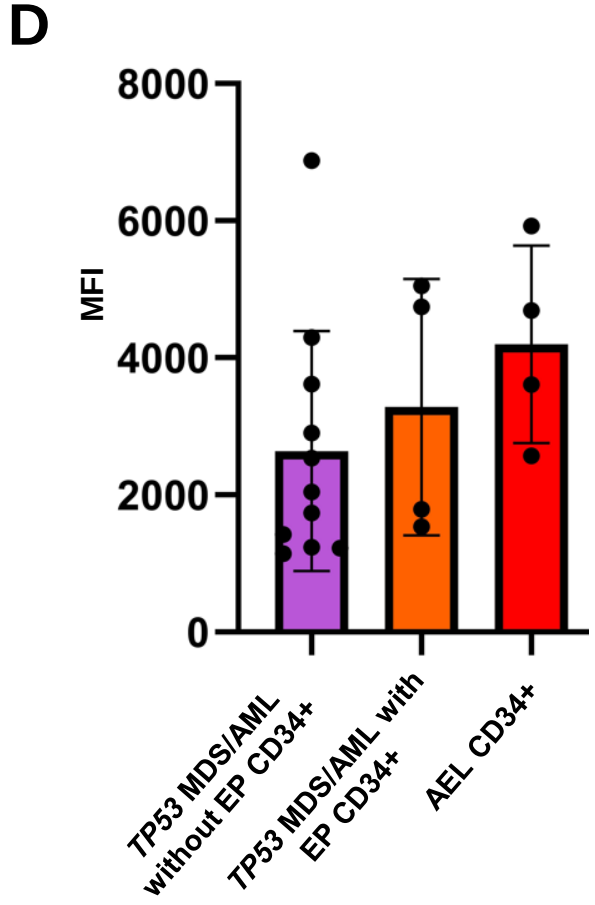


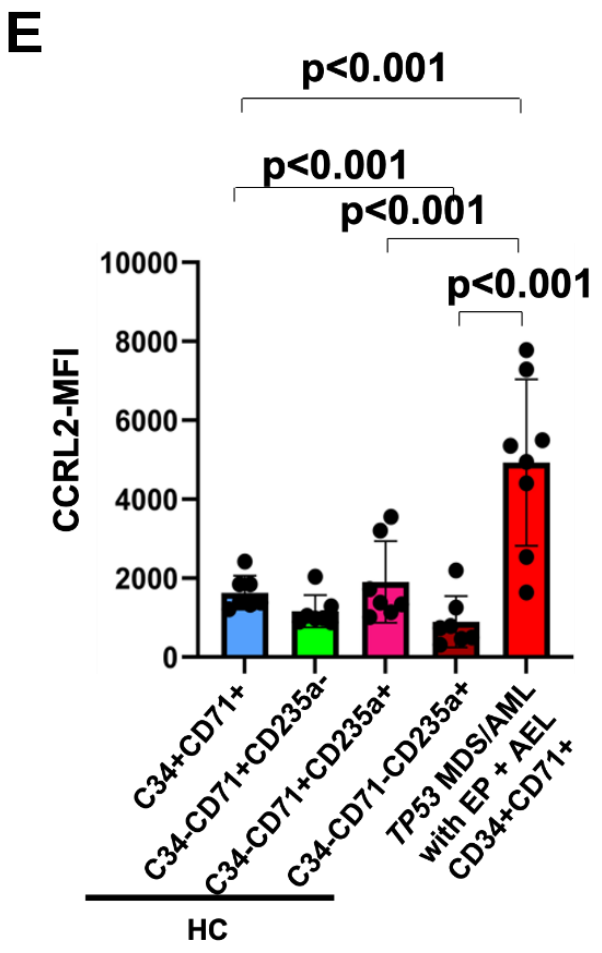


**Supplementary Figure 2**

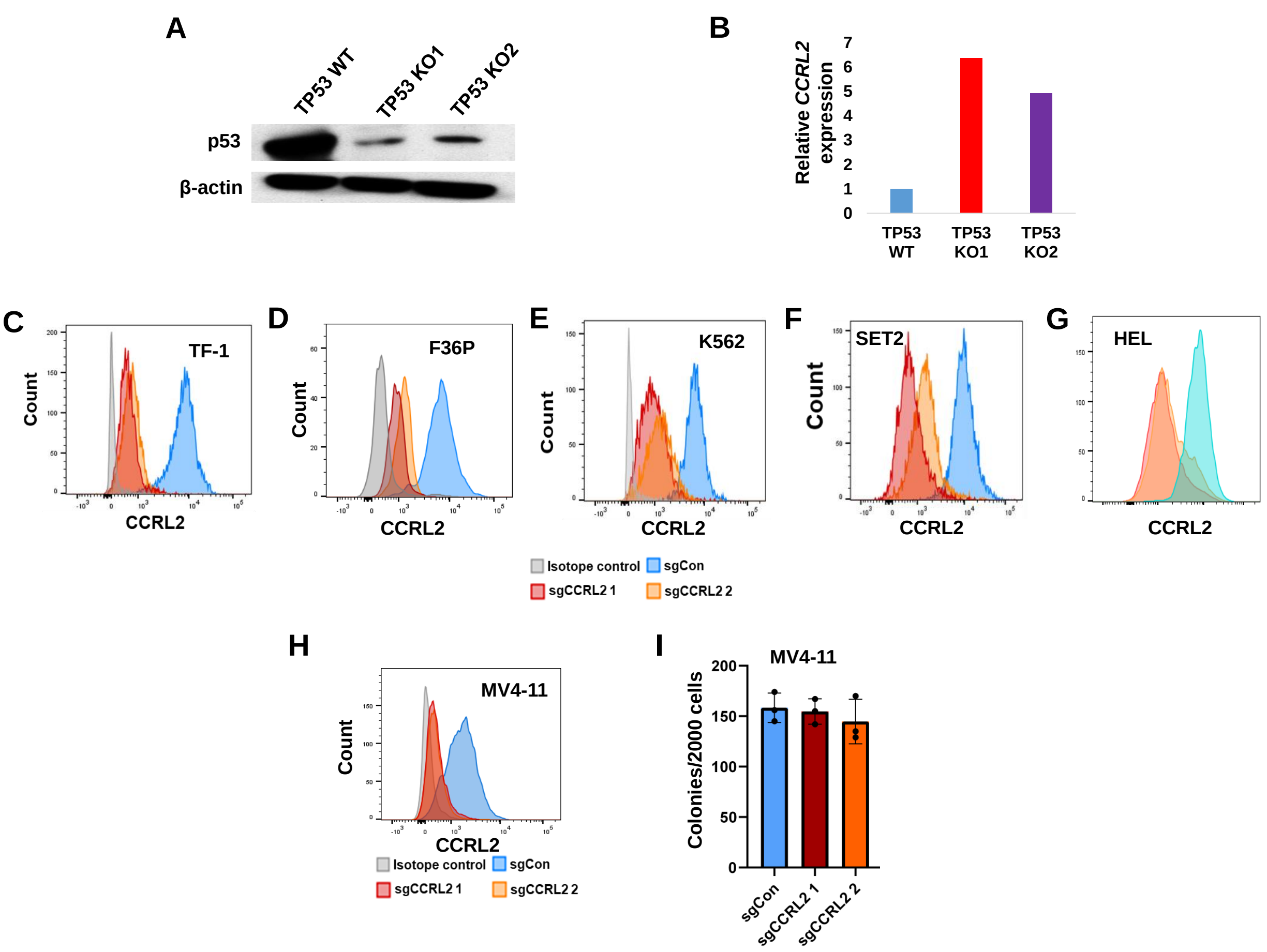


**Supplementary Figure 3**

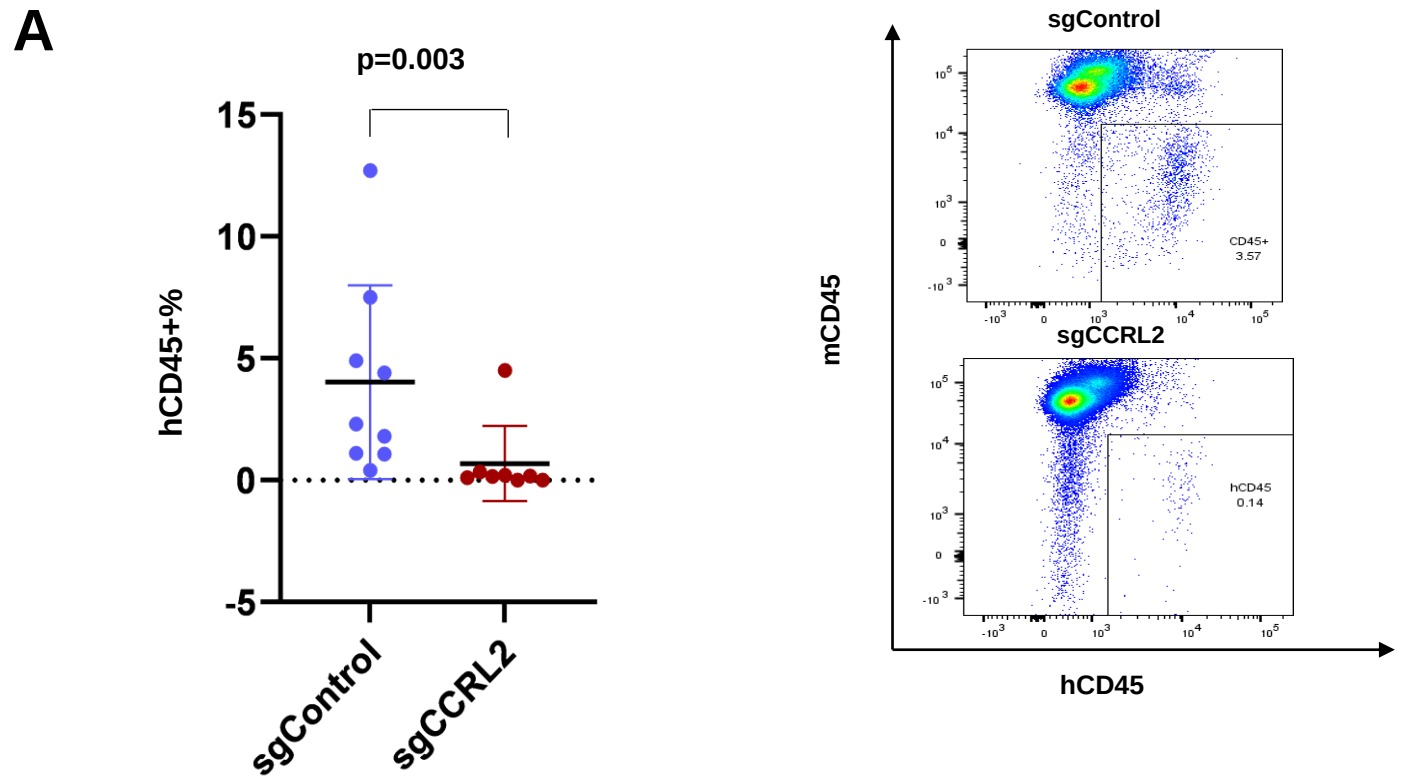


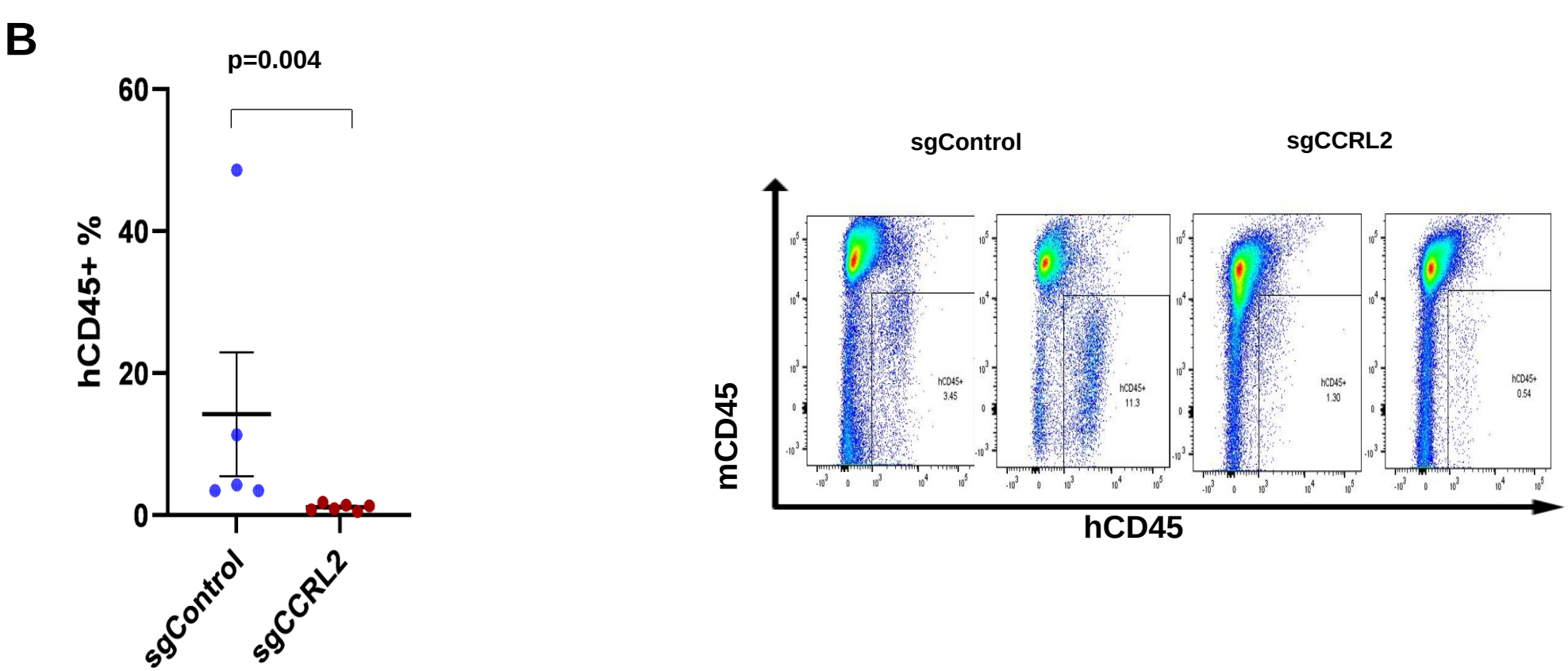


**Supplementary Figure 4**

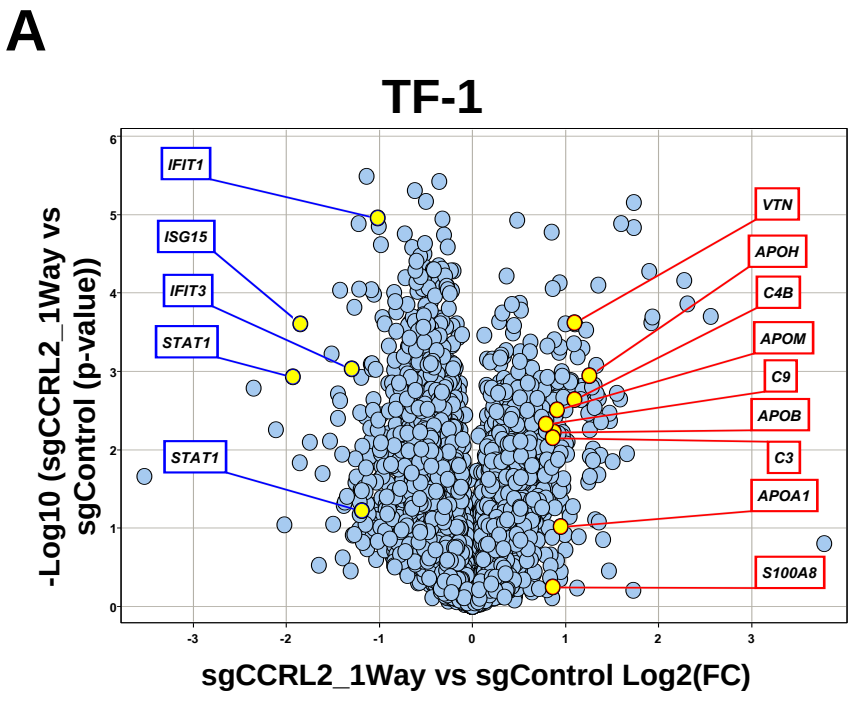


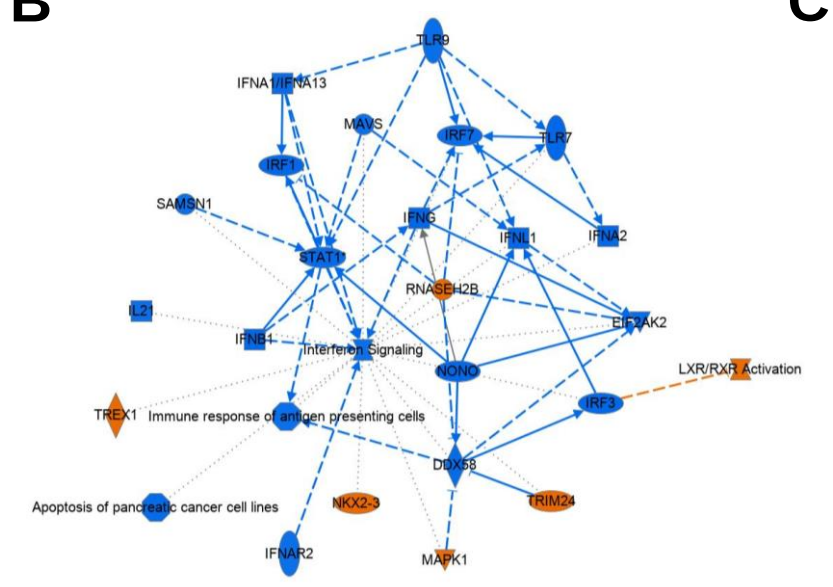


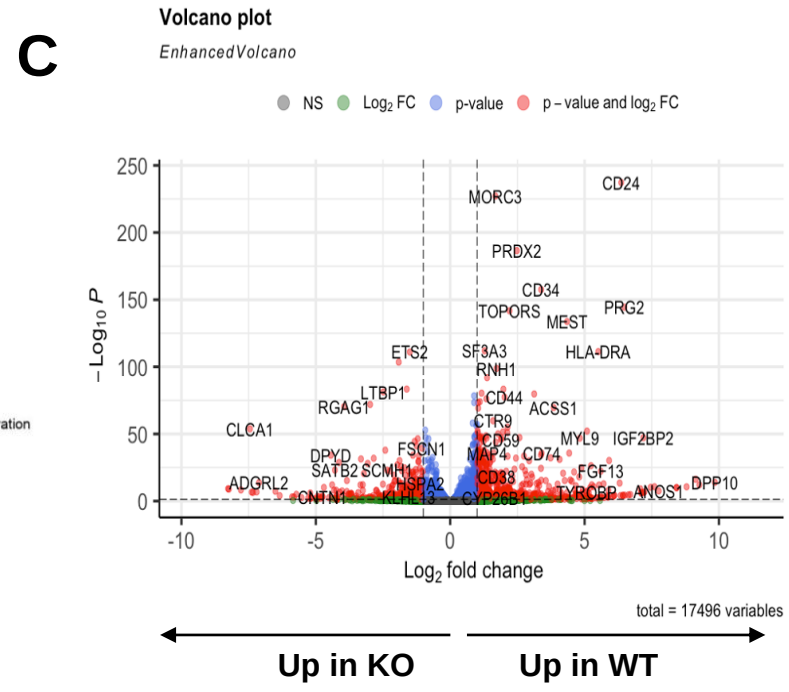


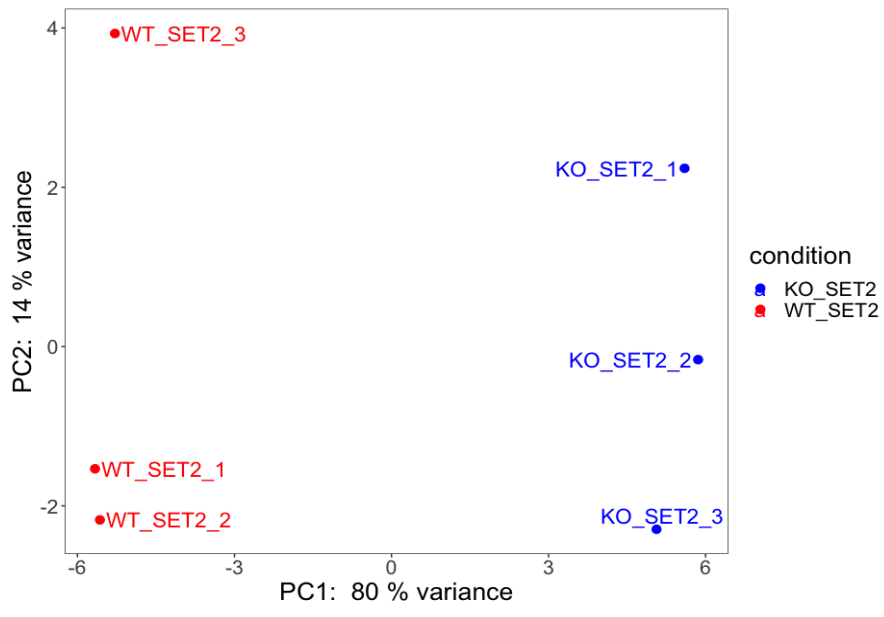


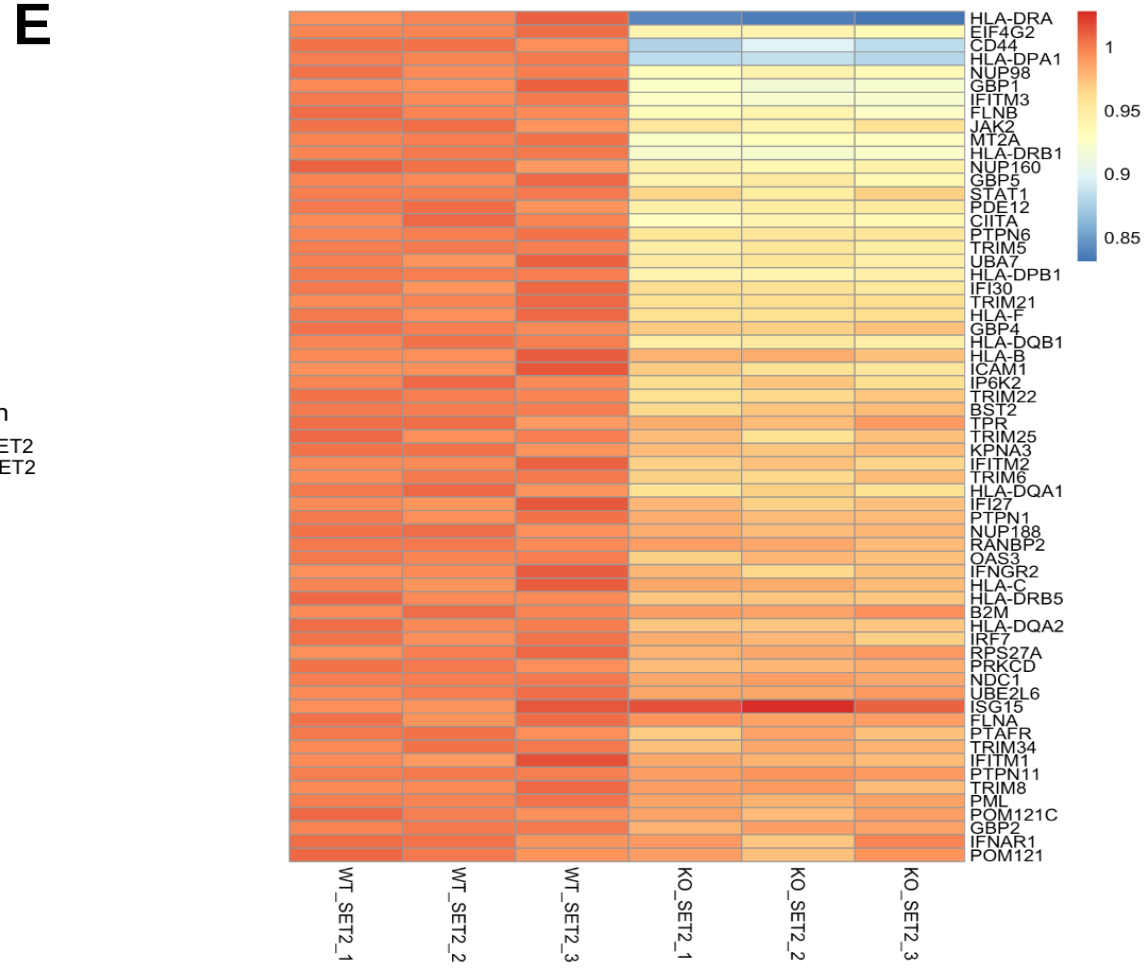


**Supplementary Figure 5**

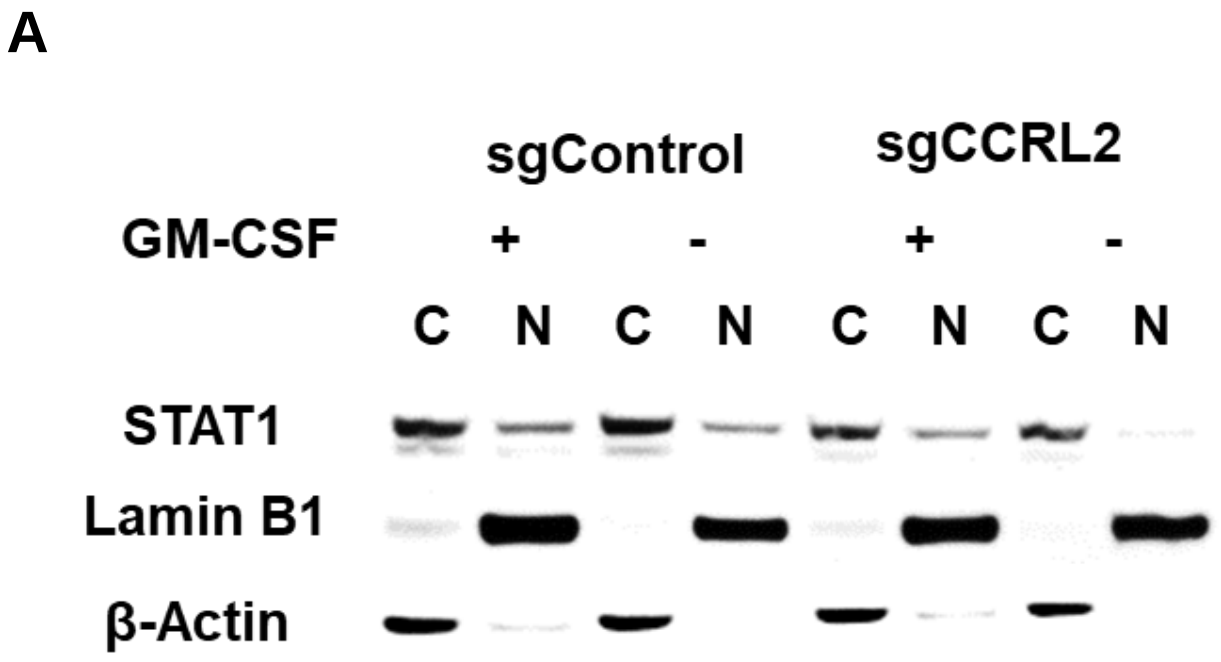


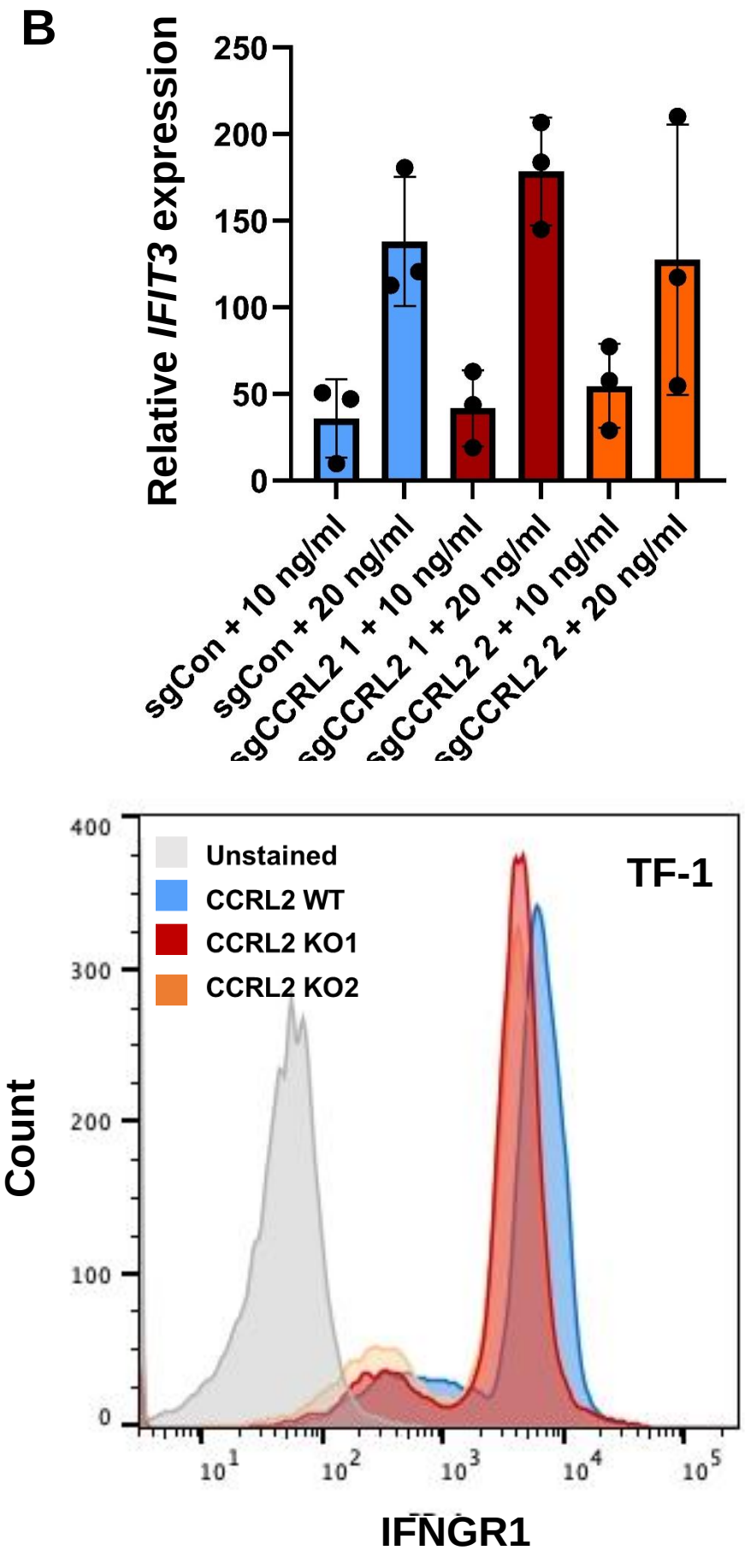


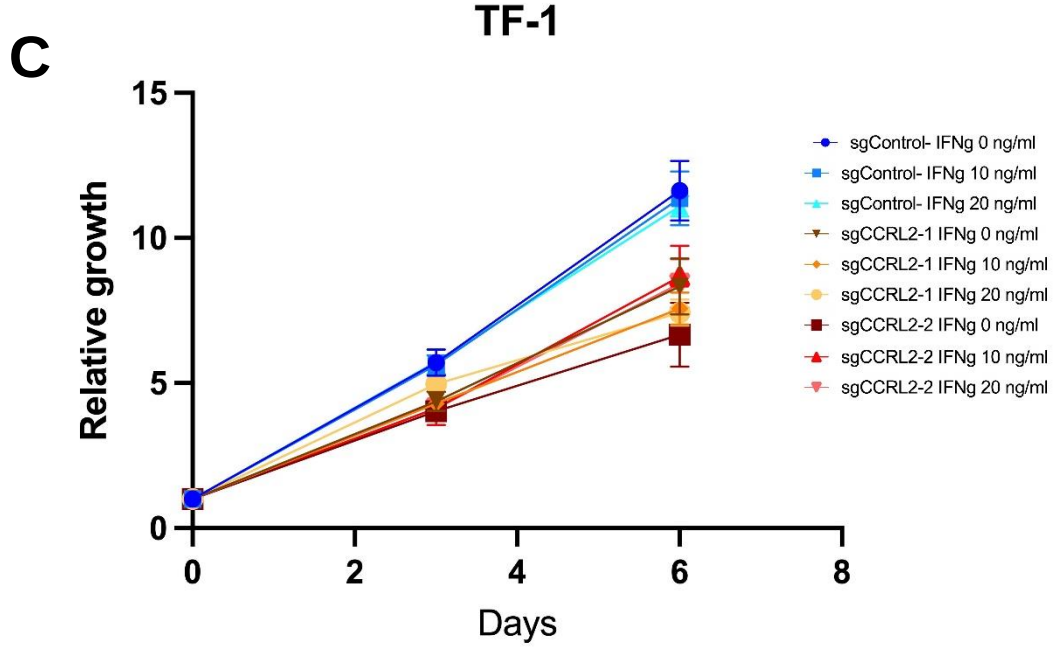





**Supplementary Figure 6**

A

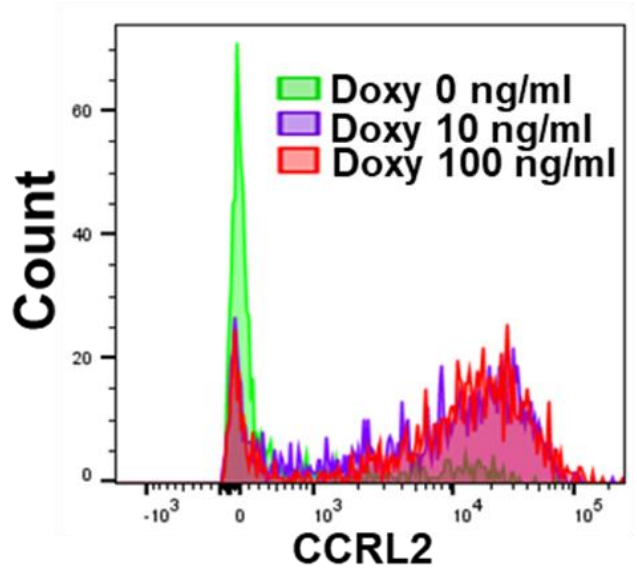


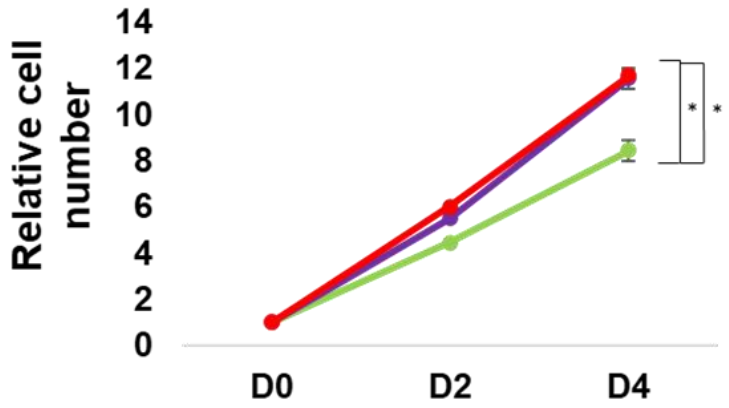


B

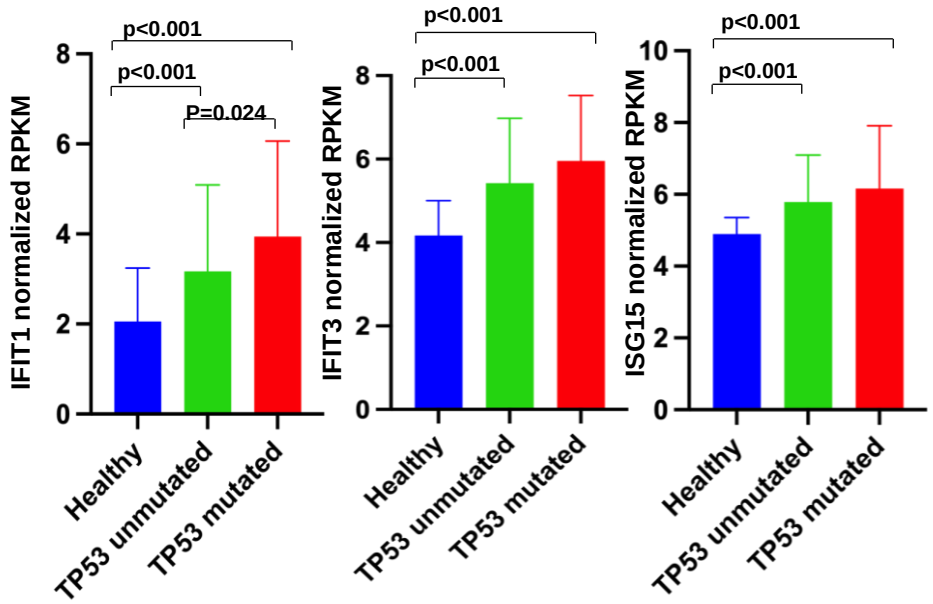


C

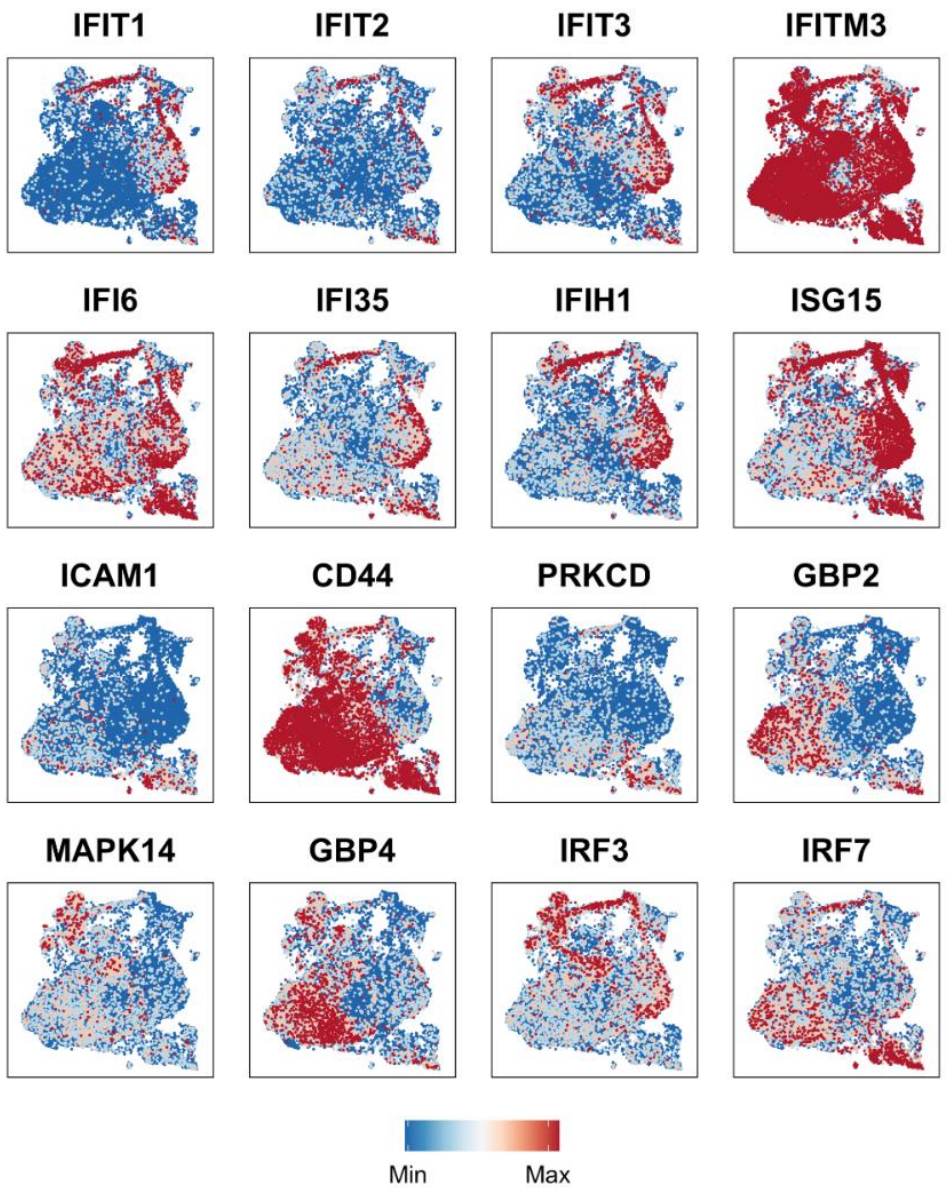


**Supplementary Figure 7**

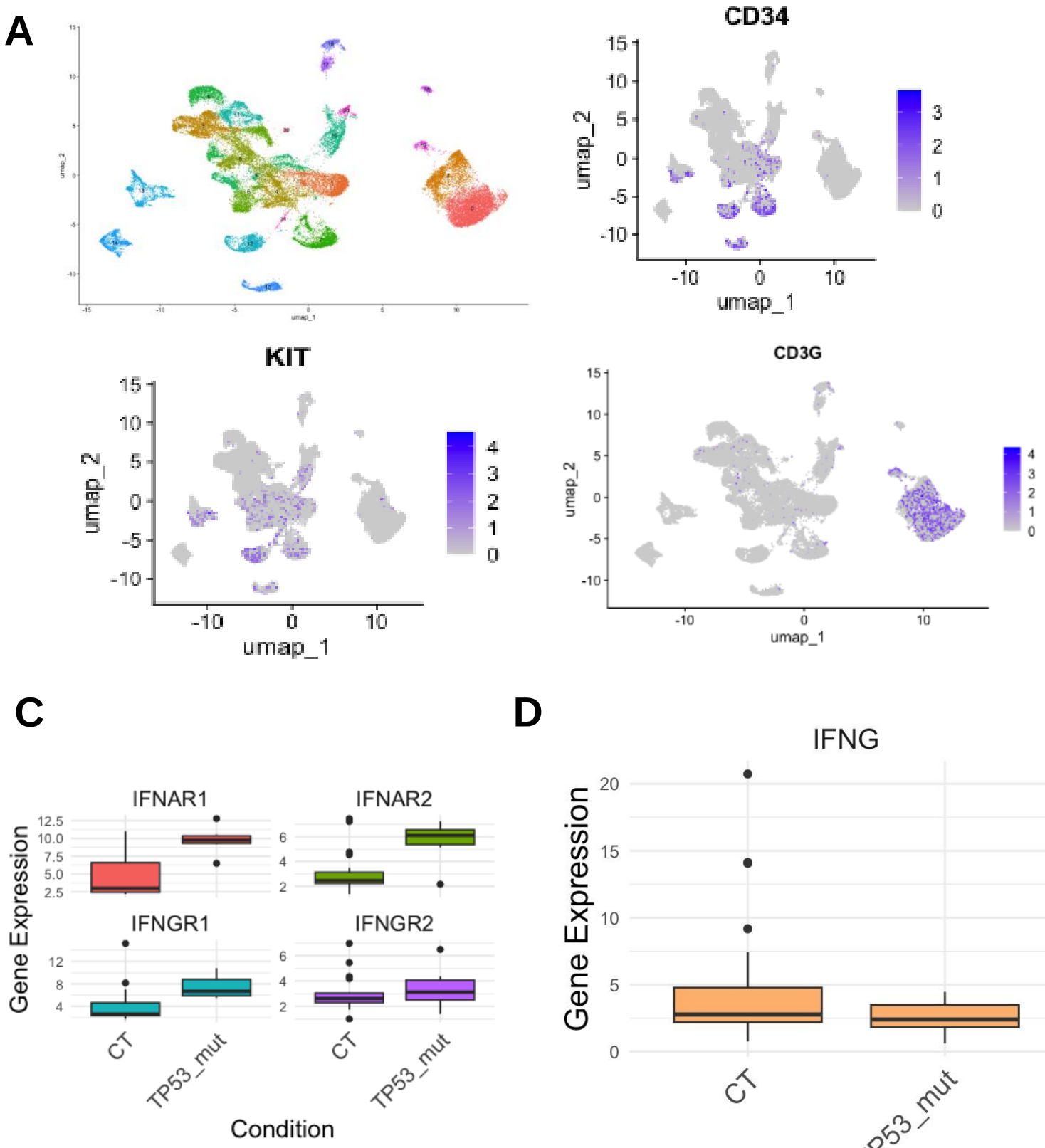


**Supplementary Figure 8**

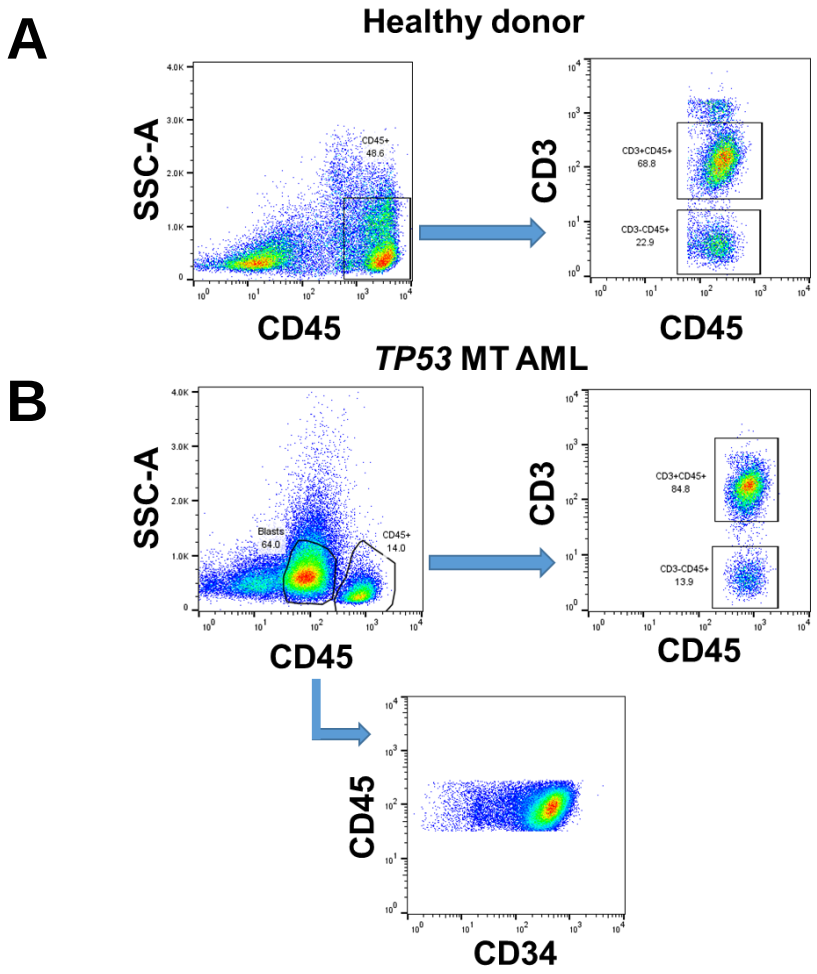


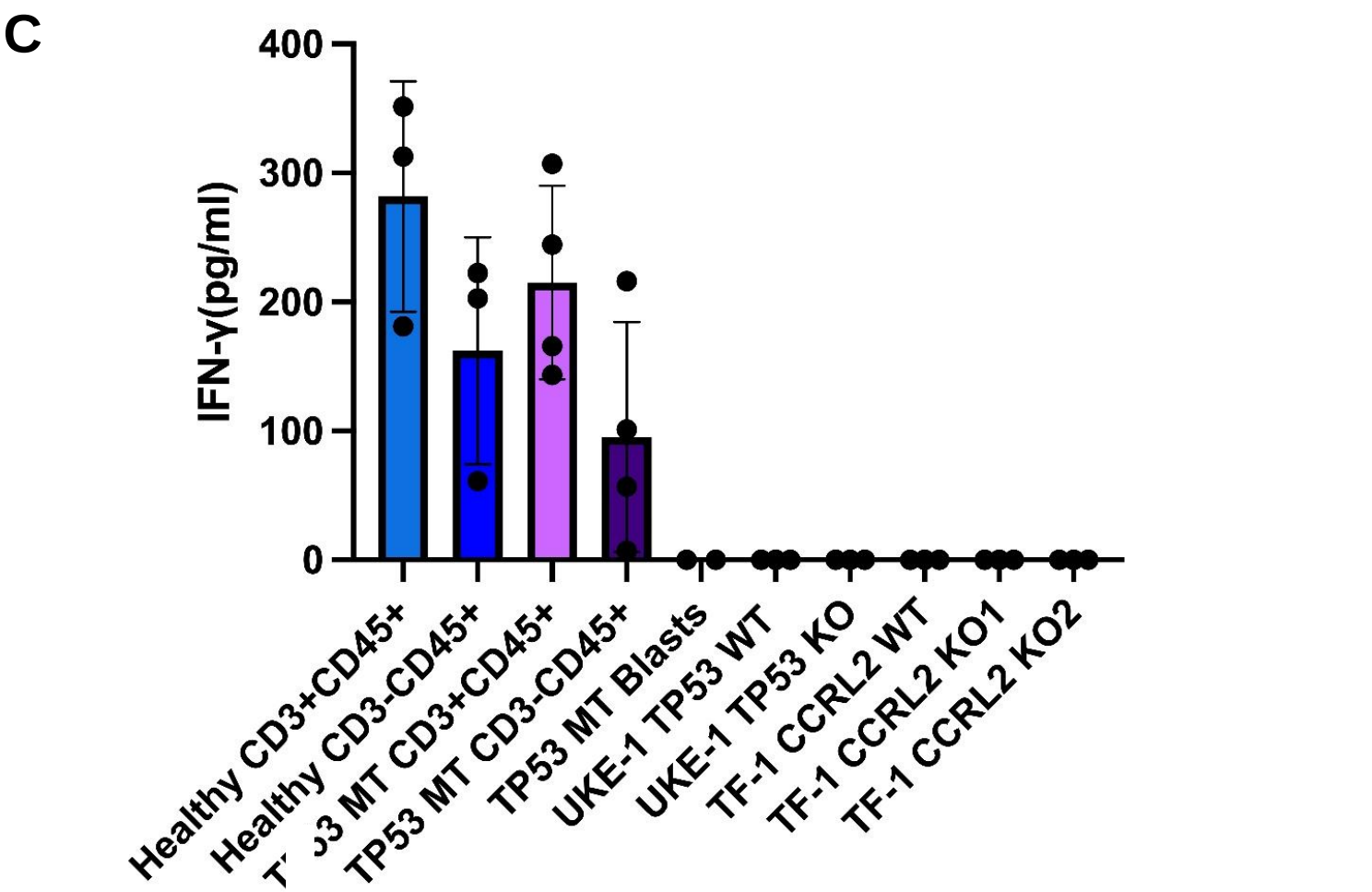


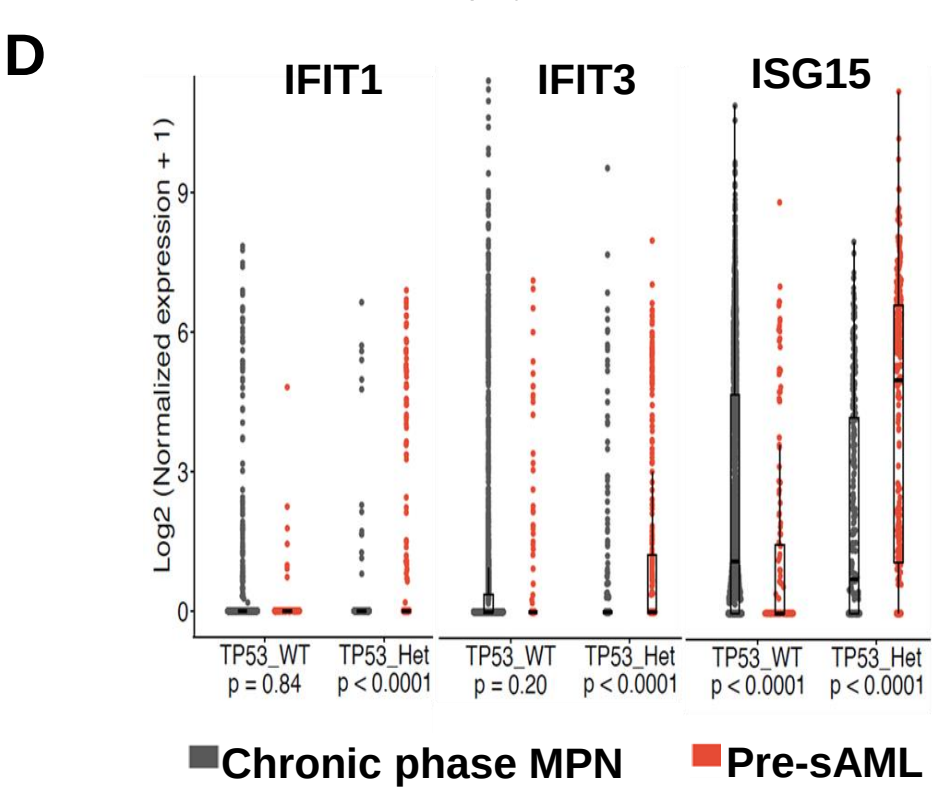


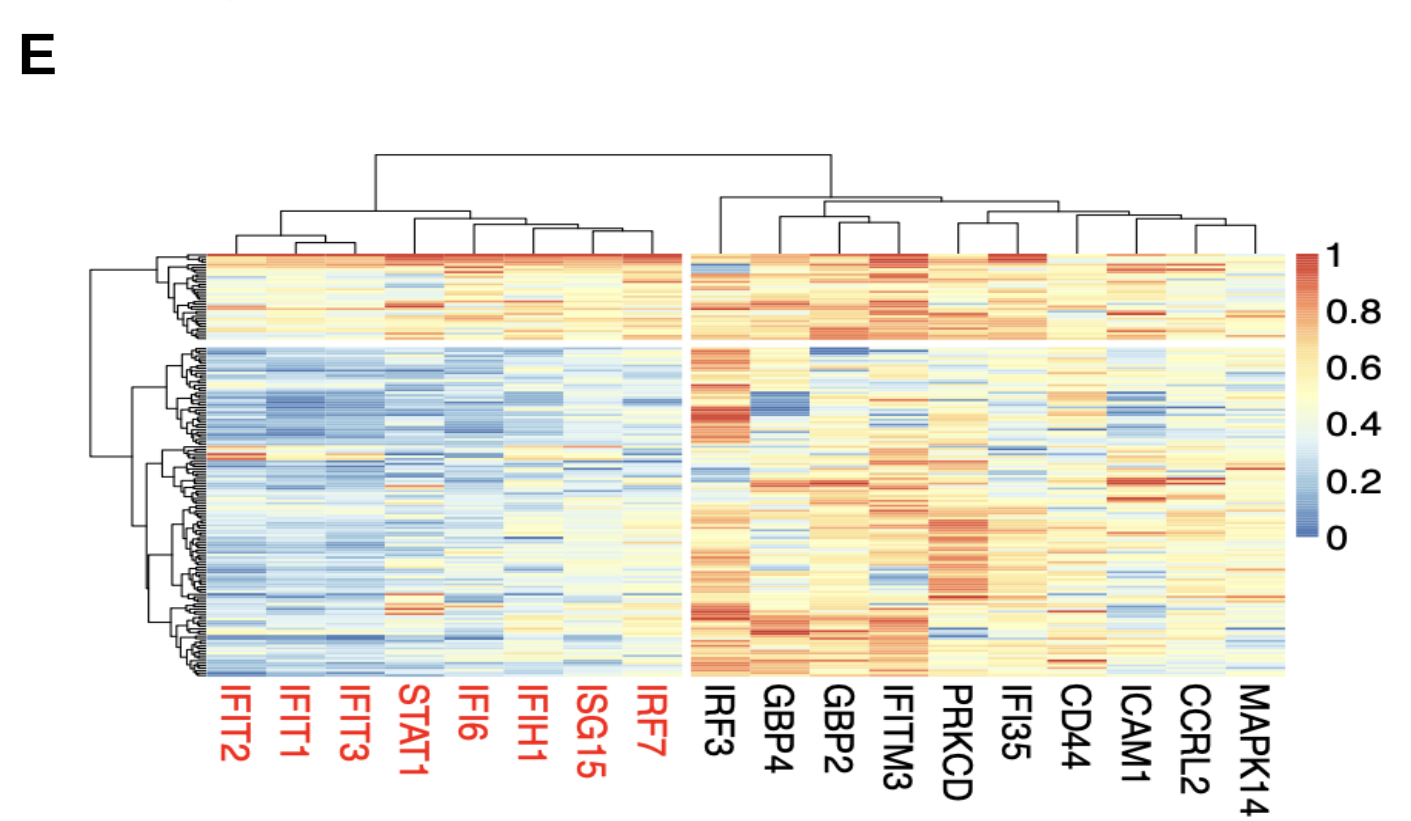


**Supplementary Figure 9**

**Supplementary Figure Legends**

**Supplementary Fig. 1. (A)** Genomic landscape of 15 patients with *TP53* MT MDS/AML with complex karyotype and either one *TP53* mutation of VAF at least 50% or two or more *TP53* mutations and 4 patients with AEL, which were included in the assessment of CCRL2 expression. 4 patients with *TP53* MT MDS/AML had erythroid predominance (EP) (≥50% of nucleated bone marrow cells were erythroid progenitors) but did not meet AEL criteria. **(B)** Lollipop plot showing specific TP53 variants of the patients' samples

**Supplementary Fig.2.** (**A)** Gating strategy for analysis of healthy donors' samples based on CD34/CD71/CD235a expression. **(B)** Gating strategy for analysis of TP53 mutated MDS/AML and AEL samples based on SSC-A/CD45 to identify blasts which express high CD71/CCRL2 (for AEL patients) and CD34/CD71 expression to identify CD34+CD71+ cells (for AEL patients). **(C-D)** *TP53* MT MDS/AML patients with EP showed a trend toward higher CCRL2 expression in their blasts and CD34+ cells respectively compared to *TP53* MT MDS/AML without EP. **(E)** Assessment of CCRL2 expression by flow cytometry in bone marrow samples of 15 patients with *TP53* MT MDS/AML with complex karyotype and either one *TP53* mutation of VAF at least 50% or two or more *TP53* mutations and 4 patients with AEL. 4 patients with *TP53* MT MDS/AML had erythroid predominance (EP) (≥50% of nucleated bone marrow cells were erythroid progenitors) but did not meet AEL criteria.

**Supplementary Fig. 3. (A)** Western blot confirming the TP53 knockouts (KO1 and KO2) in UKE-1 cells. **(B)** qPCR showing higher CCRL2 expression in *TP53* KO UKE-1 cells compared to *TP53* WT UKE-1 cells. **(C-H)** CCRL2 knockout (KO) with two different lentiviruses (sgCCRL2 1 and sgCCRL2 2) compared to scramble sgRNA (sgControl) was confirmed by flow cytometry in TF-1, F36P, K562, SET2 and HEL cells respectively. **(I)** CCRL2 KO showed no effect on the clonogenicity of the *TP53* WT monocytic MV4-11 cells.

**Supplementary Fig. 4. (A)** On day 65, survived TF-1 mice were euthanized. Disease burden in bone marrow was measured by human CD45+%. Mice engrafted with sgCCRL2 had a significantly lower percentage of human CD45+ than those engrafted with sgControl (p=0.003). **(B)** Disease burden in bone marrow of SET2 engrafted mice was measured by human CD45+%. Mice engrafted with sgCCRL2 had a significantly lower percentage of human CD45+ than those engrafted with sgControl (p=0.004).

**Supplementary Fig. 5. (A)** Volcano plot of fold changes (FC) in protein expression between CCRL2 knockout (sgCCRL2) and wild type (sgControl) cells show the IFN-γ signaling regulator STAT1 (both long and short isoforms) along with the IFN-γ targets (IFIT1, IFIT3 and ISG15) were amongst the top downregulated proteins by CCRL2 KO. LXR/RXR targets are upregulated in CCRL2 KO cells. **(B)** Protein-protein interaction network showing that CCRL2 positively regulates IFN-γ signaling and suppresses LXR/RXR activation. **(C)** Bulk RNA-seq was performed followed by gene set enrichment analysis (GSEA) using a compilation of pathways from MSigDB in CCRL2 WT or KO SET2 cells. Volcano plot portrays the expression of the differentially expressed genes. **(D)** Principal components analysis showing principal components 1 and 2 (PC1 and PC2) variances for SET2 WT and KO cells. **(E)** Heatmap shows that IFN-γ gene networks was found to be the top CCRL2-regulated pathway.

**Supplementary Fig. 6. (A)** CCRL2 KO decreased the nuclear translocation of STAT1 in TF-1 cells (C: cytoplasm, N: nucleus). **(B)** Treatment of TF-1 CCRL2 KO and WT cells with 10 ng/ml and 20 ng/ml of IFN-γ showed that CCRL2 KO had no effect on the upregulation of *IFIT3* expression as a response to exogenous IFN-γ. **(C)** Treatment of TF-1 CCRL2 WT and KO cells with two doses of IFN-γ (10 ng/ml and 20 ng/ml) showed no impact on cells growth in the presence

or absence of CCRL2 expression. **(D)** CCRL2 KO caused a modest suppression of IFN-γ receptor (IFNGR) levels in the surface of TF-1 cells in the absence of exogenous IFN-γ.

**Supplementary Fig. 7. (A)** Doxycycline (doxy)-inducible CCRL2 TF-1 cell model upon treatment with 10 or 100 ng/ml doxycycline induced CCRL2 expression and increased their growth at 2 and 4 days ($p=0.008$ for 10 ng/ml and $p=0.003$ for 100ng/ml). **(B)** Comparison of the expression of *IFIT1*, *ISG15* and *IFIT3* between *TP53* WT and *TP53* MT AML samples was done by analyzing RNA sequencing data derived from Beat AML dataset. *IFIT1* was found to be significantly overexpressed in *TP53* MT AML samples compared to *TP53* WT ones ($p=0.024$). All three CCRL2/STAT1 target genes were upregulated in AML samples compared to healthy bone marrow mononuclear cells ($p<0.001$). **(C)** Analysis of single-cell RNA sequencing data from Kuusanmäki et al. showed that blasts with erythroid differentiation express higher levels of various CCRL2/IFN-γ targets including *IFIT1*, *IFIT2*, *IFIT3*, *IFI35*, *IFIH1* and *ISG15* compared to other AML differentiation clusters.

**Supplementary Fig. 8. (A)** Analysis of single cell RNA sequencing data from van Galen et al. identified blasts from bone marrow aspirates of 16 AML patients including 3 individuals with *TP53* mutations by CD34 and c-KIT (CD117) expression and T-cells by CD3 expression. **(B)** Volcano plot showing that most of the CCRL2/IFN-γ associated genes are overexpressed in *TP53* MT AML cells compared to *TP53* WT ones. **(C)** *IFNGR1* and *IFNGR2* show a very modest upregulation in *TP53*-mutated AML samples (p-adjusted= 0.051 and 0.860 respectively) compared to blasts from *TP53* WT AML patients, as shown in the Gene expression BoxPlot. Each dot in the boxplot represents the pseudobulk aggregated expression data for one study participant normalized by a size factor as implemented in DESeq2. (**D**) Comparison of *IFNG* in T-cells of *TP53* WT and MT AML patients based on single cell RNA sequencing data from van Galen et al.

showing that patients with *TP53* MT AML did not express higher levels of *IFNG* compared to the WT ones. (**E**) *TP53* deletion in UKE-1 cells did not affect the expression of IFNGR1 in cells surface.

**Supplementary Fig.9 (A**) Sorting of CD3+CD45+ and CD3-CD45+ cells from 4 *TP53* mutated AML patients and 3 healthy bone marrow donors. **(B)** Blasts by dim CD45 and low side scatter were also sorted from the *TP53* mutated AML patients. **(C)** Cells (50,000 cells/ml) were cultured for 72 hours and levels of IFN-γ were then measured by ELISA, showing that T-cells from *TP53* MT AML cells secreted relatively lower IFN-γ levels compared to healthy donors. Blasts from TP53 mutated AML patients, UKE-1 TP53 WT and KO and TF-1 CCRL2 WT and KO cells were not found to secrete any IFN-γ. **(D)** Analysis of publicly available single-cell RNA sequencing data showed that pre-leukemic *TP53* heterozygous clones from patients with myeloproliferative neoplasms (MPN) who transformed to multi-hit *TP53* mutated sAML have higher expression of *IFIT1* ($p<0.0001$), *IFIT3 (*$p<0.0001$) and *ISG15* ($p<0.0001$) compared to *TP53* heterozygous clones from patients who remained in chronic phase (CP-MPN). **(E)** Heatmap showing the unsupervised clustering of genes and patients, considering the scaled gene expression values. Both rows and columns of the heatmap were cut in two based on dendrogram height. Through this, we separated the patients in two clusters based on the expression pattern of the CCRL2/IFN-γ targets: Cluster 2 patients ($n = 35$) who presented a high expression of *IFIT2, IFIT1, IFIT3, STAT1, IFI6, IFIH1, ISG15, IRF7*, whereas Cluster 1 patients ($n = 134$) contained the rest of the patients.

## Supplementary Methods

### Patients and sample processing

Normal marrow was collected as excess material after harvesting normal donors for allogenic bone marrow transplantation. All specimens were obtained by the Johns Hopkins Kimmel Cancer Center Specimen Accessioning Core. Isolation of CD34+ cell subsets was performed using the CD34 MicroBead kit (Miltenyi Biotec) as before[1, 2].

### Cell lines and reagents

TF-1 cells and F36P cells were cultured in RPMI 1640 (Thermo Fischer Scientific, Waltham, MA) with 10% and 20% fetal bovine serum (FBS) (MilliporeSigma, Burlington, MA) respectively with the addition of GM-CSF (2 ng/ml and 20 ng/ml respectively; PeproTech). K562 and UKE-1 cells were cultured in RPMI 1640 with 10% FBS. SET2 and HEL cells were cultured in RPMI 1640 with 10% FBS. MV4-11 cells were cultured in IMDM (Thermo Fischer Scientific, Waltham, MA) with 10% FBS. All the cell lines were cultured with 2mM L-glutamine, penicillin (100 U/ml) and streptomycin (100µg/ml) at 37 in 5% CO2. Doxycycline was purchased from Sigma Aldrich (D9891) and was diluted in PBS (Thermo Fischer Scientific, Waltham, MA).

### Flow cytometry analysis

Gating was based on an unstained control. Following staining, analysis was performed using BD LSR II (BD Biosciences). Mean fluorescence intensity (MFI) was measured for each marker using FlowJo analysis software version 10.0.8(FlowJo, Ashland, CO, USA).

### CCRL2 and TP53 knockout

TF-1, F36P, K562, SET2, HEL and MV-411 cells were incubated with the viral supernatant and polybrene (8µg/ml; MilliporeSigma) for transduction. 48 hours later, cells were treated with

puromycin (2µg/ml for TF-1 and K562, 1.5 µg/ml for F36P, 0.5 µg/ml for SET2 and HEL and 0.75 µg/ml for MV4-11) for 3-4 days for resistant cells selection.

Similarly, lentiviral vectors expressing TP53-targeting sgRNA (or empty were transfected into 293T cells as detailed above. UKE-1 cells were incubated with the viral supernatant and polybrene (8µg/ml; MilliporeSigma) for transduction. 48 hours later, cells were treated with Blasticidin (10 µg/ml) for 3-4 days for resistant cells selection.

**Colony formation assay**

Clonogenic assays were conducted as previously detailed [1, 2]. Cells were counted and resuspended at a density of 3000 cells/ml in methylcellulose-based media. Following around two weeks of incubation at 37°C in 5% CO2, counting of colony forming units was performed under bright-field microscopy.

**TF-1 and SET2 xenograft mice**

After transduction of TF-1 and SET2 cells with sgRNAs, and selection of resistant cells as above, resistant cells were transduced with a GFP/Luciferase+ retroviral vector as before [1, 2]. Afterward, GFP+ cells sorted, and injected intravenously to 8-10-week-old NOD.Cg-*Prkdc*$^{scid}$ *Il2rg*$^{tm1Wjl}$/SzJ (NSG) female mice ($10^6$ cells per mouse). Using IVIS spectrum in vivo imaging system, bioluminescence signal was measured. At day 65 for TF-1 and 60 for SET2, all remaining mice were euthanized, and the percentage of human CD45+ cells was assessed in bone marrow by flow cytometry. Our study has been performed under a mouse protocol approved by the Johns Hopkins University Animal Care and Use Committee (IACUC).

**Mass spectrometry phosphoproteomics analysis**

Protein extracts were buffer exchanged using SP3 paramagnetic beads (GE Healthcare)[3]. Briefly, protein samples (20 ug) were brought up to 100 uL with 10 mM TEAB + 1% SDS and disulfide bonds reduced with 10 uL of 50 mM dithiothreitol for 1 hour at 60C. Samples were cooled to RT and pH adjusted to ~7.5, followed by alkylation with 10 uL of 100 mM iodoacetamide in the dark at RT for 15 minutes. Next, 100 ug (2 uL of 50 ug/uL) SP3 beads were added to the samples, followed by 120 uL 100% ethanol. Samples were incubated at RT with shaking for 5 minutes. Following protein binding, beads were washed with 180 uL 80% ethanol three times. Proteins were digested on-bead with 2ng trypsin (Pierce) in 100uL 25mM TEAB buffer at 37C overnight. Resulting peptides were separated from the beads using a magnetic tube holder. Supernatants containing peptides were acidify and desalted on u-HLB Oasis plates. Peptides were eluted with 60% acetonitrile/0.1%TFA and dried using vacuum centrifugation.

Each of the 12 dried peptide samples were labeled with one of the unique TMTpro 16-plex reagents (Thermo Fisher, Lot WK338750) according to the manufacturer's instructions. All 12 TMT labeled peptide samples were combined and dried by vacuum centrifugation.

The combined TMT-labeled peptides were re-constituted in 100 µL 200mM TEAB buffer and filtered through Pierce Detergent removal columns (Fisher Scientific PN 87777) to remove excess TMT label. Peptides in the flow through were diluted to 2 mL in 10 mM TEAB in water and loaded on a XBridge C18 Guard Column (5 µm, 2.1 x 10 mm, Waters) at 250 µL/min for 8 min prior to fractionation on a XBridge C18 Column (5 µm, 2.1 x 100 mm column (Waters) using a 0 to 90% acetonitrile in 10 mM TEAB gradient over 85 min at 250 µL/min on an Agilent 1200 series capillary HPLC with a micro-fraction collector. Eighty-four 250 ul fractions were collected and concatenated into 24 fractions[4]. From each fraction, 10% was analysis for global quantitative

proteomic comparison and normalization. The remaining 90% was combined into 12 fractions for phosphopeptide enrichment by binding to titanium dioxide (TiO2)[5].

TMT labeled peptides before and after phosphopeptide enrichment were analyzed by nanoflow reverse phase chromatography coupled with tandem mass spectrometry (nLCMS/MS) on an Orbitrap-Fusion Lumos mass spectrometer (Thermo Fisher Scientific) interfaced with an EasyLC1000 UPLC. Peptides will be separated on a 15 cm × 75 μm i.d. self-packed fused silica columns with ProntoSIL-120-5-C18 H column 3 μm, 120 Å (BISCHOFF) using an 2-90% acetonitrile gradient over 85 minutes in 0.1% formic acid at 300 nl per min and electrosprayed through a 1 μm emitter tip (New Objective) at 2500 V. Survey scans (MS) of precursor ions were acquired with a 2 second cycle time from 375-1500 m/z at 120,000 resolution at 200 m/z with automatic gain control (AGC) at 4e5 and a 50 ms maximum injection time. Top 15 precursor ions were individually isolated within 0.7 m/z by data dependent monitoring and 15s dynamic exclusion and fragmented using an HCD activation collision energy 39. Fragmentation spectra (MS/MS) were acquired using a 1e5 AGC and 118 ms maximum injection time (IT) at 50,000 resolution.

Fragmentation spectra were processed by Proteome Discoverer (v2.4, ThermoFisher Scientific) and searched with Mascot v.2.8.0 (Matrix Science, London, UK) against RefSeq2021_204 database. Search criteria included trypsin enzyme, two missed cleavage, 5 ppm precursor mass tolerance, 0.01 Da fragment mass tolerance, with TMTpro on N-terminus and carbamidomethylation on C as fixed modifications and TMTpro on K, phosphorylation on S, T or Y, oxidation on M, deamidation on N or Q as variable modifications. Peptide identifications from the Mascot searches were processed within PD2.4 using Percolator at a 5% False Discovery Rate confidence threshold, based on an auto-concatenated decoy database search. Peptide spectral matches (PSMs) were filtered for Isolation Interference <25%. Relative protein abundances of

identified proteins were determined in PD2.4 from the normalized median ratio of TMT reporter ions from the top 30 most abundant proteins identified. Technical variation in ratios from our mass spectrometry analysis is less than 10% [6].

**Pathway Enrichment Analysis**

The raw grouped values were then transformed to log2 notation and the wild-type and knock-down values were then quantile normalized to reduce experimental noise across the three biological replicates each. A t-test analysis was then run to compare the two, WT and KO, biological classes by relative abundance, expressed as fold change, and statistical significance, expressed as p-value. Proteins that demonstrated >2SD absolute value fold change were judged to be differentially abundant, and all these results were exported to the Ingenuity Pathway Analysis (QIAGEN Inc.) platform for functional analysis.

Ingenuity Pathway Analysis, IPA, evaluated its known pathways to determines those that are enriched for proteins that demonstrated this >2SD fold change, by comparing each pathway's number of proteins that do or do-not not show this fold change. For each specific pathway IPA returned a Fisher's exact test of whether an enrichment exists, and a Z-score whether the pathway is likely inhibited or activated.

**Western Blotting**

Protein extraction was performed using M-PER™ Mammalian Protein Extraction Reagent (#78501). Antibodies against P-STAT1 ($Tyr^{701}$) (#9167), P-STAT1 ($Ser^{727}$) (#9177), STAT1(#9172), and ßactin (#4970) were all purchased from Cell Signaling Technology.

**Co-immunoprecipitation**

Cell lysates from TF-1, F36P, SET2 cells and doxy-inducible CCRL2 TF-1 cells were incubated overnight with Sepharose bead conjugate JAK2 monoclonal antibody (Cell Signaling Technology,

#4089) or Sepharose bead conjugate isotype control (Cell Signaling Technology, #3423) as previously described[1]. Beads were then washed extensively and boiled with 30 µl of loading buffer.

**Single cell RNA sequencing analysis**

Publicly available single cell RNA sequencing data from Kuusanmaki et al. was preprocessed as previously described [7]. Gene expression was visualized using Seurat (v5.1.0) and scCustomize (v2.0.1) in R (v4.3.1). The heatmap pertaining to this analysis was generated using ComplexHeatmap(v2.16.0).

Another publicly available single cell RNA sequencing data from van Galen et al. [28]. Gene expression was visualized using Seurat (v5.1.0) (PMID 29608179) and in R (v4.3.1). Briefly, the single cell data across samples were merged. The UMI matrix was then normalized for library size, log transformed and scaled. Principal Component Analysis (PCA) was performed followed by Louvain nearest neighbor clustering using 30 PCs. UMAP was applied to visualize the cell distribution in 2D space. A resolution of 0.5 was used for clustering to identify different cell populations. Cluster identity was identified using canonical marker genes. Differential expression (DE) analysis in individual clusters across groups of samples was performed using a pseudobulk approach. Specifically, counts across cells for each sample were aggregated using the AggregateExpression function. Surrogate variable analysis (SVA) was applied to identify latent confounders (PMID 22257669) and differential expression was estimated using DESeq2 v1.44.0 (PMID 25516281) with surrogate variables as covariates. FDR < 0.05 was set as the significance threshold.

**Bulk RNA sequencing**

We followed the DESeq2 pipeline (PMID 25516281) to normalize the gene expression results using a size factor that accounts for library size and gene size. This was followed by a variance stabilizing transformation as implemented in DESeq2, the output of which was used to perform principal components analysis (PCA). Surrogate variable analysis (SVA) was employed to control for unknown confounders and batch effects (PMID 22257669) while preserving the biological differences between groups. Differential expression (DE) was tested based on a Wald test with a two-tailed alternative hypothesis and a corresponding p-value was generated and adjusted for multiple testing using false discovery rate (FDR). Genes were considered significant if their FDR was $< 0.05$. The gene set enrichment analysis (GSEA) package was used to identify pathways enriched in our DE results (PMID 16199517).

**Quantitative real-time PCR**

Quantitative real-time polymerase chain reaction (PCR) was performed as previously described[8]. Total RNA was extracted using the Monarch Total RNA miniprep kit(T2010S) and complementary DNA was synthesized using QuantiTect Rev. Transcription Kit (#205311, Qiagen, Valencia, CA). Quantitative real-time PCR was conducted by using sequence-specific primers. The Radiant SYBR Green Lo-ROX qPCR kit (Alkali Scientific, Fort Lauderdale, FL) and CFX96 real-time PCR detection system (Bio-Rad) were utilized. Normalization of RNA expression was based on GAPDH expression.

**Nuclear and cytoplasmic Fractionation**

Nuclear/cytoplasmic fractionation was performed using the NE-PER$^{TM}$ Nuclear and Cytoplasmic Extraction Kit (ThermoFischer Scientific #78833) as previously described[9].

**Publicly available databases**

Analysis of the mRNA levels of *CCRL2* and STAT1 target genes (*IFIT1, ISG15 and IFIT3*) in different subtypes of AML was based on RNA sequencing data derived from The Cancer Genome ATLAS (TCGA). Clinical and transcriptomic data in the form of RSEM values from the TCGA LAML cohort were downloaded via cBioPortal[10-12]. Only samples that had transcriptomic and FAB information available were included. Patients were grouped based on their FAB status in M6/7 and M1/2/3/4/5, the latter being labelled as "Other". A total of 171 patients from the TCGA were included. Of those, 5 (2.9%) had an FAB of M6/7. Normality of the distribution of the RSEM values was assessed using skewness and kurtosis assessment and histogram visualization. Differences between two non-normally distributed groups were evaluated using the Mann-Whitney-Wilcoxon rank sum test. A p-value under 0.05 was considered statistically significant. We calculated an overall CCRL2/IFN signaling score based on TCGA dataset using an 18 gene list: RSEM values for CCRL2, STAT1, IFIT1, ICAM1, CD44, IFIT2, PRKCD, IFIT3, IFI35, ISG15, GBP2, IFIH1, MAPK14, GBP4, IFI6, IRF3, IRF7, IFITM3 were min max scaled at the gene level. To obtain a score for every patient, we took the median of these scaled values at the patient level. Similarly, data was extracted from DepMap Portal (DepMap22Q2). TPM values for CCRL2, STAT1, IFIT1, ICAM1, CD44, IFIT2, PRKCD, IFIT3, IFI35, ISG15, GBP2, IFIH1, MAPK14, GBP4, IFI6, IRF3, IRF7, IFITM3 were min max scaled at the gene level. To obtain a score for every patient, we took the median of these scaled values at the cell line level. Using Beat AML dataset, data was extracted from http://vizome.org/aml/expression_strat/. Patients were included if DxAtSpecimenAcquisition was Acute Myeloid Leukaemia (AML) and related

precursor neoplasms or Healthy, pooled CD34+. Patients were included if Included_2018_DNAseqAnalysis was y or Healthy; pooled CD34+ and if none of the 18 included genes had n/a in the Normalized_RPKM column. A total of 407 patients were included. Of those, 12 (2.9%) were healthy CD34+, 360 (88.5%) were TP53 WT AML and 35 (8.6%) were TP53 MUT AML.Values from the RPKM_normalized column for CCRL2, STAT1, IFIT1, ICAM1, CD44, IFIT2, PRKCD, IFIT3, IFI35, ISG15, GBP2, IFIH1, MAPK14, GBP4, IFI6, IRF3, IRF7, IFITM3 were min max scaled at the gene level. To obtain a score for every patient, we took the median of these scaled values at the patient level. For overall survival using TCGA dataset, the surv_cutpoint function from the survminer package was used to determine an optimal cutoff for the CCRL2/IFN signaling score when it comes to overall survival. A patient was considered to have a high CCRL2/IFN signaling score if this score was over 0.1332826. The optimal cutoff for the RSEM values were 127.4210 for CCRL2, 161.9048 for IFIT1, 132.8000 for IFIT3, and 213.1177 for ISG15.

To determine specific expression differences (*CCRL2*, *IFIT1*, *IFIT3* and *ISG15*) between different CP-MPNs genotypes that progressed to sAML (pre-TP53-sAML) and that did not (CP-TP53-MPN), we used a previously published dataset[13]. Normalized gene expression per cell were downloaded from GSE226340 while corresponding genotyping data was downloaded from https://doi.org/10.5281/zenodo.8060602,metadata_MPNAMLp53_with_index_genotype.revised.txt.Normality of the distribution was assessed using histogram visualization and kurtosis and skewness evaluation. Differences between two non-normally distributed groups were assessed using Mann-Whitney-Wilcoxon rank sum test. Similarly, RNA expression data from DepMap Portal was analyzed to compare gene expression between different AML cell lines and data derived

from Beat AML database was used to compare the expression of CCRL2, and STAT1 targets across AML samples based on molecular profile.

For data on the effect of IFN on venetoclax resistance, we included 169 patients. If a patient presented multiple samples, we included the sample with the lower ID number. We focused on the expression of the following genes: CCRL2, STAT1, IFIT1, ICAM1, CD44, IFIT2, PRKCD, IFIT3, IFI35, ISG15, GBP2, IFIH1, MAPK14, GBP4, IFI6, IRF3, IRF7, IFITM3. The expression values were min max scaled at a gene level. The CCRL2 Signaling Score was defined at a patient level and was considered as the median scaled expression level of the included genes. Correlation between the CCRL2 Signaling Score and Venetoclax IC50 was assessed using Spearmans rho. Unsupervised clustering and its graphical representation was performed using the pheatmap package (https://github.com/raivokolde/pheatmap), using ward.D2 clustering. Mann-Whitney-Wilcoxon rank sum test was used to determine the difference in Venetoclax IC50 between Cluster 1 and 2.

**Statistical Analysis**

Statistical analysis was performed by using GraphPad Prism (GraphPad Software, La Jolla, CA). Mann-Whitney test was performed to assess statistical significance when comparing two groups. One-way analysis of variance (ANOVA) was performed for the comparisons of three or more groups. Dunnett's test was used for multiple comparisons. Standard deviation was used to assess centrality and dispersion.

## References


1. Karantanos, T., et al., *The role of the atypical chemokine receptor CCRL2 in myelodysplastic syndrome and secondary acute myeloid leukemia*. Sci Adv, 2022. **8**(7): p. eabl8952.
2. Karantanos, T., et al., *CCRL2 affects the sensitivity of myelodysplastic syndrome and secondary acute myeloid leukemia cells to azacitidine*. Haematologica, 2023. **108**(7): p. 1886-1899.
3. Hughes, C.S., et al., *Single-pot, solid-phase-enhanced sample preparation for proteomics experiments*. Nat Protoc, 2019. **14**(1): p. 68-85.
4. Wang, Y., et al., *Reversed-phase chromatography with multiple fraction concatenation strategy for proteome profiling of human MCF10A cells*. Proteomics, 2011. **11**(10): p. 2019-26.
5. Larsen, M.R., et al., *Highly selective enrichment of phosphorylated peptides from peptide mixtures using titanium dioxide microcolumns*. Mol Cell Proteomics, 2005. **4**(7): p. 873-86.
6. Herbrich, S.M., et al., *Statistical inference from multiple iTRAQ experiments without using common reference standards*. J Proteome Res, 2013. **12**(2): p. 594-604.
7. Kuusanmäki, H., et al., *Erythroid/megakaryocytic differentiation confers BCL-XL dependency and venetoclax resistance in acute myeloid leukemia*. Blood, 2023. **141**(13): p. 1610-1625.
8. Chang, Y.T., et al., *Role of CYP3A4 in bone marrow microenvironment-mediated protection of FLT3/ITD AML from tyrosine kinase inhibitors*. Blood Adv, 2019. **3**(6): p. 908-916.
9. Hung, S.C., et al., *Angiogenic effects of human multipotent stromal cell conditioned medium activate the PI3K-Akt pathway in hypoxic endothelial cells to inhibit apoptosis, increase survival, and stimulate angiogenesis*. Stem Cells, 2007. **25**(9): p. 2363-70.
10. Gao, J., et al., *Integrative analysis of complex cancer genomics and clinical profiles using the cBioPortal*. Sci Signal, 2013. **6**(269): p. pl1.
11. Cerami, E., et al., *The cBio cancer genomics portal: an open platform for exploring multidimensional cancer genomics data*. Cancer Discov, 2012. **2**(5): p. 401-4.
12. Weinstein, J.N., et al., *The Cancer Genome Atlas Pan-Cancer analysis project*. Nat Genet, 2013. **45**(10): p. 1113-20.
13. Rodriguez-Meira, A., et al., *Single-cell multi-omics identifies chronic inflammation as a driver of TP53-mutant leukemic evolution*. Nat Genet, 2023. **55**(9): p. 1531-1541.

**Supplementary Table 1.** Characteristics of patients with *TP53* mutated myeloid neoplasms and healthy donors

| **Characteristic** | ***TP53* mutated myeloid neoplasms (N=19)** | **Healthy donors (N=16)** |
|---|---|---|
| Age | 65 (27 – 78) | 44 (30 – 56) |
| Gender<br>Females<br>Males | <br>4 (21%)<br>15 (79%) | <br>6 (37.5%)<br>10 (62.5%) |
| Diagnosis<br>*TP53* mutated MDS/AML<br>AEL | <br>15 (79%)<br>4 (21%) | N/A |
| Treatment-related | 6 (32%) | N/A |
| Blasts% | 25 (5-80) | N/A |
| Karyotype<br>Complex | <br>19 (100%) | N/A |

**Supplementary Table 2.** Variants and variant allele frequencies of patients with *TP53* mutated myeloid neoplasms.

| Variant(s) | VAF1 | VAF2 |
|---|---|---|
| R158H | 79.9 | |
| Y126H | 81.9 | |
| D281N | 20.64 | |
| H178P | 82.41 | |
| Y220C, R158H | 24.5 | 26.7 |
| G245S | 67.5 | |
| F270C | 89.9 | |
| Y220C | 64.1 | |
| V272M | 60.5 | |
| R175H | 50.3 | |
| c.994-1G>A | 85.24 | |
| D281N | 97.54 | |
| C275Y | 52.56 | |
| S303fs | 86.5 | |
| V272M | 69.14 | |
| R196P | 50.2 | |
| R273H, E285fs | 15.98 | 14.4 |
| H179R | 79.3 | |
| E286G, R273H | 37.83 | 36.07 |